Letter

# Effective model and $s_{\pm}$-wave superconductivity in trilayer nickelate $La_4Ni_3O_{10}$

Qing-Geng Yang,[1,*] Kai-Yue Jiang,[2,*] Da Wang,[1,3,†] Hong-Yan Lu,[2,‡] and Qiang-Hua Wang[1,3,§]

[1]*National Laboratory of Solid State Microstructures and School of Physics, Nanjing University, Nanjing 210093, China*

[2]*School of Physics and Physical Engineering, Qufu Normal University, Qufu 273165, China*

[3]*Collaborative Innovation Center of Advanced Microstructures, Nanjing University, Nanjing 210093, China*

(Received 16 February 2024; revised 26 May 2024; accepted 13 June 2024; published 26 June 2024)

The recent discovery of bulk superconductivity in trilayer nickelate $La_4Ni_3O_{10}$ under high pressure is attracting a new wave of research interest. In this Letter, we study its electronic band structure and construct a minimal trilayer tight-binding model in terms of the nickel $3d_{x^2-y^2}$ and $3d_{3z^2-r^2}$ orbitals, and investigate the superconducting mechanism due to local Coulomb interactions by the unbiased functional renormalization group. We find antiferromagnetic correlations between the outer layers instead of neighboring ones, apart from the in-plane correlations. The effective interaction induces Cooper pairing with the $s_{\pm}$-wave symmetry, which changes sign across the Fermi pockets. In addition, we find the $T_c$ in $La_4Ni_3O_{10}$ is systematically lower than that in $La_3Ni_2O_7$, but electron doping can further enhance $T_c$.

DOI: 10.1103/PhysRevB.109.L220506

*Introduction*. As important progress in pursuing high-temperature superconductivity with a perovskite structure other than cuprates, the discovery of bilayer Ruddlesden-Popper (RP) $La_3Ni_2O_7$ (La327) with a critical temperature $T_c$ near 80 K under high pressure [1] has attracted significant attention both experimentally [2–25] and theoretically [26–60]. Since the average electronic configuration of the nickel atom is $3d^{7.5}$, both $3d_{x^2-y^2}$ and $3d_{3z^2-r^2}$ orbitals are active ones near the Fermi level. In this material, the superconductivity is now generally attributed to the strong vertical interlayer coupling between the nickel $3d_{3z^2-r^2}$ orbitals, leading to an extended $s$-wave (also called $s_{\pm}$-wave) pairing [27,29,30,37–39,41,49–51,58,59], although there are also some other proposals [43–48,54,61]. Such a picture is quite different from cuprates or infinite-layer nickelates, which have the atomic configuration of Cu or Ni near $3d^9$ and hence can be described by the effective single-orbital model [62,63].

At the present stage, the superconducting volume fraction of La327 samples appears to be very small [14], asking for further refinement of the samples. In fact, the bilayer RP phase appears to coexist with another alternated single-triple-layer ("1313") RP phase [17–19]. Interestingly, the trilayer RP $La_4Ni_3O_{10}$ (La4310) is also reported recently to show signatures of superconductivity [5–7,53] and zero resistance [8] under high pressure above 43 GPa. The maximum $T_c$ of La4310 (reaching up to 30 K) is lower than La327, while its superconducting volume fraction is found to be very high [8], indicating the superconductivity in La4310 is a bulk property rather than filamentary as in the present-stage La327 [14]. There are some similarities between the two systems. La4310 has a nominal chemical valence $Ni^{2.67+}$, in favor of a mixed $3d^7$ and $3d^8$ electronic configuration as in La327. La4310 also undergoes a structural transition from monoclinic $P2_1/a$ to tetragonal $I4/mmm$ space group at pressures around 12–20 GPa [8,10,53], together with the change of the $c$-axis Ni-O-Ni bond angle into 180°. The superconductivity only occurs in the high-pressure tetragonal phase. There is, however, a marked difference between the two families: The La4310 has three layers, and the inner one is inequivalent to the outer ones. It is a timely and important issue to investigate the pairing mechanism and pairing symmetry of La4310, and to understand how it is related to La327.

In this Letter, we construct a minimal trilayer tight-binding model with the nickel $3d_{3z^2-r^2}$ and $3d_{x^2-y^2}$ orbitals for La4310 in the high-pressure tetragonal phase from *ab initio* calculations on the basis of first-principle calculations. We then investigate the electronic correlation effect from two-orbital Coulomb interactions using the unbiased singular-mode functional renormalization group (SM-FRG) [27,64–66]. We find the spin fluctuations exhibit a peculiar antiferromagnetic coupling between the two outer layers, which subsequently induces the $s_{\pm}$-wave superconductivity with the dominant pairings between $3d_{3z^2-r^2}$ orbitals both in the inner plane and between the two outer planes rather than neighboring ones. Our results show the $T_c$ of La4310 is systematically lower than that of La327, setting La327 as the most promising candidate for high-$T_c$ in the RP families of nickelates.

*Tight-binding model*. For the trilayer RP La4310 under high pressure with the tetragonal lattice structure shown in Fig. 1(a), we first perform density functional theory (DFT) calculations by the Vienna *ab initio* simulation package (VASP) [67]. The crystal structure parameters with the $I4/mmm$ space group at 40 GPa are adopted [10]. The projector augmented-wave (PAW) [68] method and the generalized gradient approximation (GGA) of the Perdew-Burke-Ernzerhof (PBE) [69] exchange-correlation functional are adopted. The plane-wave cutoff energy is set as 500 eV. The Γ-centered $12\times12\times12$ and $36\times36\times36$ $k$-point grids (in the tilted

*These authors contributed equally to this work.
†Contact author: dawang@nju.edu.cn
‡Contact author: hylu@qfnu.edu.cn
§Contact author: qhwang@nju.edu.cn

 

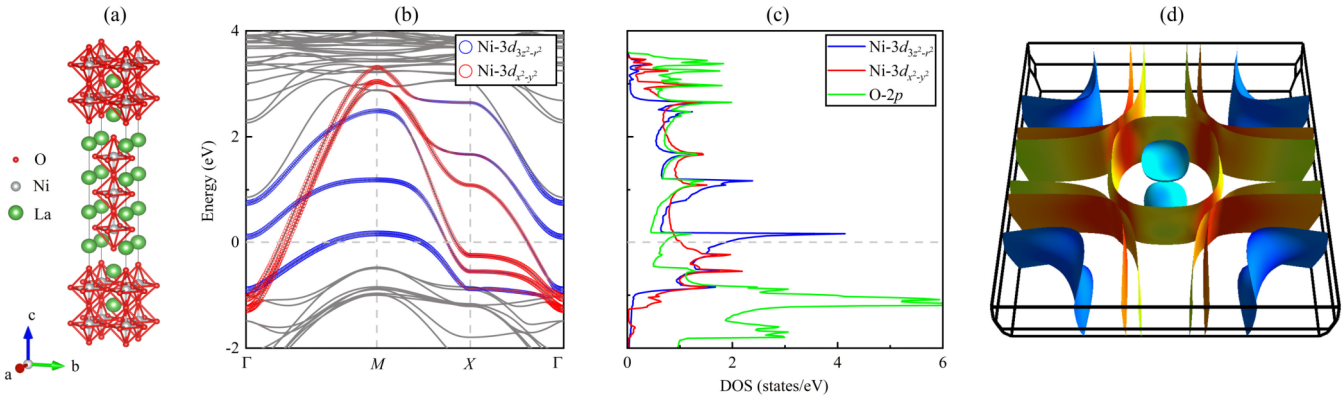


FIG. 1. (a) Crystal structure, (b) orbital-projected band structure, (c) partial DOS, and (d) three-dimensional Fermi surface of La4310 in the high-pressure tetragonal phase.

equilateral Brillouin zone) are used for the self-consistent and density of states (DOS) calculations, respectively. Combining the orbital-projected band structure and partial DOS as shown in Figs. 1(b) and 1(c), it is evident that the states near the Fermi level ($E_F$) are dominated by nickel $3d_{x^2-y^2}$ and $3d_{3z^2-r^2}$ orbitals, which is consistent with the chemical valence analysis and similar to La327 [1,26,28–30,59]. In Fig. 1(d), we show the three-dimensional Fermi surface. The four sheets of large Fermi surfaces are found to be roughly two-dimensional-like, except the additional small Fermi sphere enclosing $(0, 0, \pi)$.

Subsequently, the maximally localized Wannier functions [70,71] with $d_{x^2-y^2}$ and $d_{3z^2-r^2}$ symmetries centering at each Ni atom are extracted by the state-of-the-art WANNIER90 [72] to construct a trilayer two-orbital tight-binding model

$$H_0 = \sum_{i\delta,ab,\sigma} t_\delta^{ab} c_{ia\sigma}^\dagger c_{i+\delta b\sigma} + \sum_{ia\sigma} \varepsilon_a c_{ia\sigma}^\dagger c_{ia\sigma}, \qquad (1)$$

where $t_\delta^{ab}$ is the hopping matrix element between the $a$ orbital on site $i$ and the $b$ orbital on site $i+\delta$, $\sigma$ denotes spin, and $\varepsilon_a$ is the on-site energy of the $a$ orbital. In the following, we use $x/z$ to denote the $3d_{x^2-y^2}/3d_{3z^2-r^2}$ orbital for simplicity. Up to $D_{4h}$ symmetry operations, the on-site energy and hopping parameters are listed in Table I. It is found that the vertical interlayer hopping $t^{zz}_{(00\frac{1}{2})} = -0.684$ eV between the $z$ orbitals is the strongest, which is similar to that in La327 [26,29,30]. On the other hand, the crystal-field splitting $\varepsilon_x - \varepsilon_z$ for both the inner (0.057 eV) and outer (0.179 eV) layers is smaller than that in La327 (0.367 eV) [26,29,30,59], indicating the two orbitals are more degenerate in La4310.

With these tight-binding parameters, we plot the band structure in Fig. 2(a) together with the DFT band at $k_z = 0$ for comparison. The Fermi level is tuned to achieve the average filling $\langle n \rangle = 1.33$ per Ni atom. Note that the tight-binding Fermi level is slightly higher than DFT since the $z$-directional dispersion has been neglected. The Fermi surface of the tight-binding model is plotted in Fig. 2(b), exhibiting four Fermi pockets. The electronlike $\alpha$ pocket around $\Gamma$ and the holelike $\gamma$ pocket around $M$ are mainly contributed by $x$ and $z$ orbitals, respectively, similarly to the case in La327. On the other hand, the single $\beta$ pocket in La327, contributed by both orbitals, now splits into two, which we label as $\beta$ and $\beta'$, respectively. Due to the mirror symmetry with respect to the inner plane, we can use its parity $P_z$ to label the different bands and Fermi pockets. As shown in Fig. 2(b), all of the $\alpha$, $\beta$, and $\gamma$ pockets are $P_z$ even, and the $\beta'$ pocket is $P_z$ odd. For the latter, the Bloch wave function by symmetry is $(1, 0, -1)$ in the (top, middle, bottom) layer basis and hence is only contributed by outer layers. This is a marked feature not shared by La327.

*Electronic correlation effect*. We now investigate the electronic correlation effect from the atomic multiorbital Coulomb interactions

$$H_I = \sum_{i,a<b,\sigma\sigma'} \left(U' n_{ia\sigma} n_{ib\sigma'} + J_H c_{ia\sigma}^\dagger c_{ib\sigma} c_{ib\sigma'}^\dagger c_{ia\sigma'}\right) + \sum_{ia} U n_{ia\uparrow} n_{ia\downarrow} + \sum_{i,a\neq b} J_P c_{ia\uparrow}^\dagger c_{ia\downarrow}^\dagger c_{ib\downarrow} c_{ib\uparrow}, \qquad (2)$$

where $U$ is the intraorbital Hubbard repulsion, $U'$ is the interorbital Coulomb interaction, $J_H$ is the Hund's coupling, and $J_P$ is the pair hopping interaction. They are assumed to respect the Kanamori relations $U = U' + 2J_H$ and $J_H = J_P$ [73]. We use the constrained random phase approximation to estimate the characteristic value of $U$ to be in the range of 2–4 eV, so that the correlation is moderate. We use the

TABLE I. On-site energies $\varepsilon_a$ and hopping integrals $t_\delta^{ab}$ of the trilayer two-orbital tight-binding model for La4310 at 40 GPa. Here, $x/z$ denotes the $3d_{x^2-y^2}/3d_{3z^2-r^2}$ orbital, I/O denotes the inner/outer layer. Note that the interlayer distance is denoted by $\frac{1}{2}$. The energy is in units of eV.

| I-$\varepsilon_x$ | I-$\varepsilon_z$ | O-$\varepsilon_x$ | O-$\varepsilon_z$ | |
|---|---|---|---|---|
| 1.116 | 1.059 | 0.858 | 0.676 | |
| I-$t^{xx}_{(100)}$ | I-$t^{zz}_{(100)}$ | O-$t^{xx}_{(100)}$ | O-$t^{zz}_{(100)}$ | |
| −0.507 | −0.158 | −0.507 | −0.146 | |
| I-$t^{xz}_{(100)}$ | I-$t^{xx}_{(110)}$ | O-$t^{xz}_{(100)}$ | O-$t^{xx}_{(110)}$ | |
| 0.282 | 0.063 | 0.275 | 0.069 | |
| $t^{zz}_{(00\frac{1}{2})}$ | $t^{xx}_{(00\frac{1}{2})}$ | $t^{zz}_{(001)}$ | $t^{xz}_{(10\frac{1}{2})}$ | $t^{zz}_{(10\frac{1}{2})}$ |
| −0.684 | 0.004 | −0.087 | −0.039 | 0.036 |

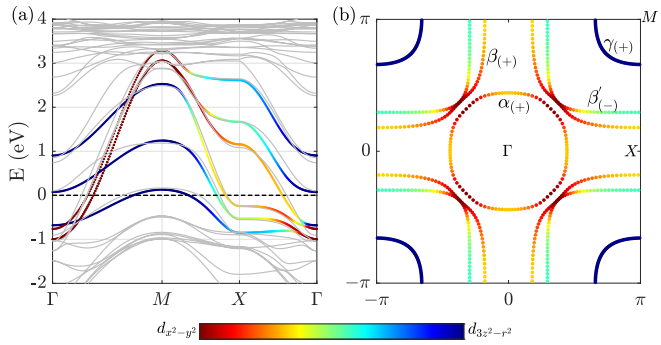


FIG. 2. (a) Band structure and (b) Fermi surfaces obtained from the tight-binding model. The DFT band at $k_z = 0$ (gray lines) is shown for comparison. The orbital weights are represented by colors and the $z$-reflection parities $P_z$ are indicated as the subscripts of the pocket names.

SM-FRG to study the effective four-point one-particle irreducible vertices $\Gamma$ flowing against the running energy scale $\Lambda$. The technical details can be found in Refs. [27,64–66]. At each $\Lambda$, the effective interactions $V_{\text{eff}}$ in the spin-density-wave (SDW), charge-density-wave (CDW), and superconductivity (SC) channels are extracted from the four-point vertices $\Gamma$. The leading singular values $S$ of these effective interactions (as scattering matrices in the fermion bilinear basis) are monitored during the RG flow. The first divergence of $S$ out of all channels indicates the instability toward an electronic order characterized by the singular bilinear scattering mode, and the divergence energy scale is characteristic of the transition temperature $T_c$.

In Fig. 3(a), we plot the inverse of the leading negative singular values $S$ vs $\Lambda$ in the three channels, respectively, at $U = 3$ eV and $J_H = 0.5$ eV. At high-energy scales, the SDW channel dominates. As $\Lambda$ decreases, it grows up but saturates at low-energy scales due to the lack of perfect Fermi-surface nesting. Instead, the SC channel is too weak and out of the view field at high-energy scales, as the bare Coulomb interaction is repulsive. But as $\Lambda$ decreases to order of the bandwidth, it is enhanced quickly as the SDW channel rises. Eventually, $1/S$ in the SC channel continues to grow logarithmically even if the other channels tend to saturate, a result of the standard Cooper mechanism. In the above sense, one could say the SC is induced by SDW fluctuations, as found also in La327.

In Fig. 3(a1), we plot the momentum $\mathbf{q}$ dependence of the leading negative singular value $S(\mathbf{q})$ in the SDW channel. Up to symmetry, there are two peaks at $q_1$ and $q_2$. Interestingly, we find the leading scattering modes at $q_1$ and $q_2$ are dominated by the antiferromagnetic arrangement of the outer-plane spins, as sketched in Fig. 3(b1), in addition to the in-plane correlations given by the corresponding plane wave $\mathbf{e}^{i\mathbf{Q}\cdot\mathbf{r}}$, where $\mathbf{Q}$ is the respective wave vector (up to equivalent ones by symmetry). Such an interesting outer-layer antiferromagnetic correlation is also obtained in another two recent theoretical works [74,75], and has actually been experimentally observed in La4310 at ambient pressure [76]. These antiferromagnetic correlations exist even in the bare spin susceptibility, and can be significantly enhanced by the Coulomb interactions due to the fact that the outer layers have less vertical hopping paths.

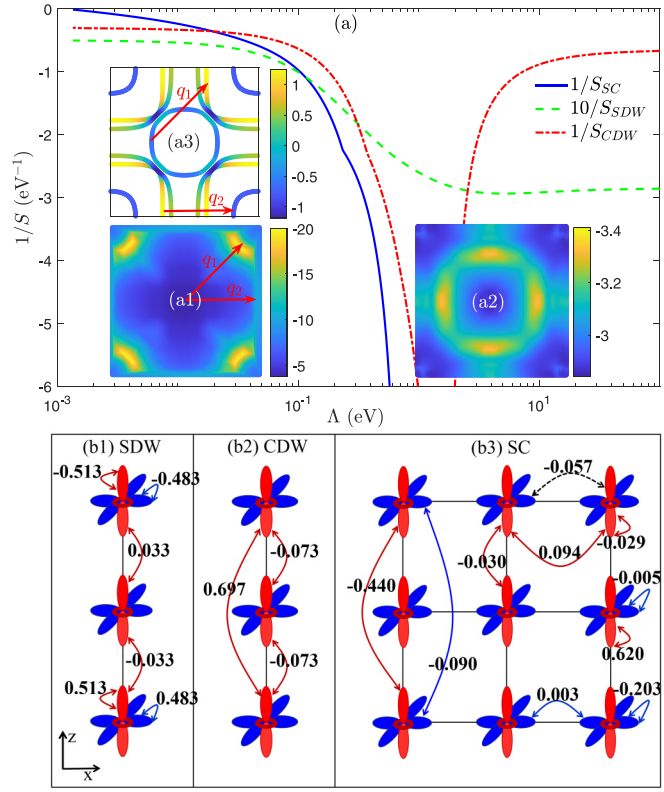


FIG. 3. (a) FRG flows of the inverse of the leading negative $S$ vs $\Lambda$ in the three channels, respectively. The $\mathbf{q}$ dependence of $S$ in the SDW and CDW channels are plotted in (a1) and (a2), respectively. The SC gap function on the Fermi surface is plotted in (a3). (b1) and (b2) shows the intra-unit-cell structure of the SDW and CDW patterns, respectively. From unit cell to unit cell, the pattern (not shown) simply transforms as the plane wave $\mathbf{e}^{i\mathbf{Q}\cdot\mathbf{r}}$, where $\mathbf{Q}$ is the respective wave vector (up to equivalent ones by symmetry). (b3) shows the real-space pattern of the leading pairing mode. Not all components are shown, but the missing ones and the spatial structure out of the view field are easily recovered by the $D_{4h}$ point group symmetry and the unit-cell-wise translation.

Note the spin structure is very different to the near-plane antiferromagnetic spin coupling in La327.

From Fig. 3(a), the CDW channel is initially reduced at high-energy scales because of the screening of charge density-density interactions. At lower-energy scales, it rises again, and we find it corresponds to the scattering of nonlocal fermion bilinears. In particular, at the final stage of the RG flow, the almost featureless $\mathbf{q}$ dependence of $S(\mathbf{q})$ is shown in Fig. 3(a2), and the bilinear is mainly composed of $z$ orbitals on the outer planes as schematically plotted in Fig. 3(b2). This is a valence bond correlation consistent with the spin coupling between the outer planes discussed above.

In the SC channel, and from the singular scattering mode, we find the pairing is a spin singlet and belongs to the $A_{1g}$ representation of the $D_{4h}$ group. The pairing operator can be written explicitly as

$$H_\Delta = \sum_{amn\mathbf{k}} \left[\Delta^{aa}_{0,mn} + \Delta^{aa}_{1,mn} f_{1+}(\mathbf{k})\right] c^\dagger_{ma,\mathbf{k}\uparrow} c^\dagger_{na,-\mathbf{k}\downarrow} + \Delta^{a\bar{a}}_{1,mn} f_{1-}(\mathbf{k}) c^\dagger_{ma,\mathbf{k}\uparrow} c^\dagger_{n\bar{a},-\mathbf{k}\downarrow} + \text{H.c.}, \quad (3)$$

where $m/n$ denotes the layer index (1–3 from top to bottom), $a$ denotes the $x/z$ orbital, $\bar{x} = z$ and $\bar{z} = x$, and $f_{1,\pm}(\mathbf{k}) = 2\cos k_x \pm 2\cos k_y$. For $U = 3$ eV and $J_H = 0.5$ eV, we find the coefficients (up to a global scale) $\Delta^{zz}_{0,22} = 0.620$, $\Delta^{zz}_{0,13} = \Delta^{zz}_{0,31} = -0.440$, $\Delta^{xx}_{0,11} = \Delta^{xx}_{0,33} = -0.203$, $\Delta^{zz}_{0,11} = \Delta^{zz}_{0,33} = -0.029$, $\Delta^{zz}_{1,11} = \Delta^{zz}_{1,33} = 0.094$, $\Delta^{xx}_{1,11} = \Delta^{xx}_{1,33} = 0.003$, $\Delta^{xz}_{1,11} = \Delta^{zx}_{1,11} = \Delta^{xz}_{1,33} = \Delta^{zx}_{1,33} = -0.057$, $\Delta_{0,12} = \Delta_{0,21} = \Delta_{0,32} = \Delta_{0,23} = -0.030$, etc. The pairing pattern is sketched in Fig. 3(b3). The pairings not shown can be obtained by $D_{4h}$ and translation symmetries. For the $A_{1g}$ pairing symmetry, since $z$ and $x$ orbitals carry different representations ($A_{1g}$ and $B_{1g}$), only intraorbital pairings are allowed for intra-unit-cell ones $\Delta^{aa}_{0,mn}$, which turn out to be much stronger than inter-unit-cell ones $\Delta^{ab}_{1,mn}$. In particular, the strongest intra-unit-cell components are $\Delta^{zz}_{0,22}$ between $z$ orbitals in the inner layer, and the vertical interlayer pairing $\Delta^{zz}_{0,13} = \Delta^{zz}_{0,31}$ between two outer layers as a result of the dominant antiferromagnetic coupling between the top and bottom layers as shown above. Here, the large value of $\Delta^{zz}_{0,22}$ is allowed for the intermediate strength of $U$ (order of bandwidth), although it is expected to vanish in the large $U$ limit. We further project the pairing function onto the band basis to obtain the gap function $\Delta_{n\mathbf{k}} = \langle n, \mathbf{k}| \sum_\delta \Delta_\delta e^{i\mathbf{k}\cdot\boldsymbol{\delta}} |n, \mathbf{k}\rangle$ where $|n, \mathbf{k}\rangle$ is the Bloch state for band $n$, $\Delta_\delta$ is understood as a matrix in the orbital-layer basis, and we have used time-reversal symmetry $T$ for $|n, -\mathbf{k}\rangle = T|n\mathbf{k}\rangle$ to eliminate the numerical phase ambiguity. The gap function on the Fermi surfaces is shown (with color scale) in Fig. 3(a3). The symmetry is evidently an extended $s$ wave or $s_\pm$ wave, similar to many theoretical proposals in La327. Both $\alpha$ and $\gamma$ pockets are fully gapped with the same sign. The gap function on the $\beta$ and $\beta'$ pockets are largely of opposite sign, although within a pocket it changes sign near the nodal direction. The SDW vectors (arrows) turn out to connect opposite gap signs on the Fermi surfaces, consistent with the spin-fluctuation scenario for singlet pairing. The gap amplitude and gap sign change on the Fermi pockets can be checked in future experiments. On the other hand, we find the subleading pairing is $d_{x^2-y^2}$-wave dominated by interorbital pairings between the outer layers. However, as the leading pairing channel diverges, the subleading one is finite and would diverge by extrapolation at a much lower-energy scale. We should point out that the RG flow drives the system into strong coupling, unlike the approaches designed in the weak-coupling limit, where there would be nearly degenerate pairing channels, but the extrapolation of which to finite coupling is not guaranteed, given the complexity of the quantum many-body effects in correlated systems.

*Phase diagram*. We have scanned the Hund's coupling $J_H$ by fixing $U = 3$ eV to obtain the phase diagram as shown in Fig. 4(a). The results of La327 are also presented for comparison. In both systems, larger $J_H$ enhances the SC until it drives the systems into the SDW state. Interestingly, for the same interaction parameters, we find the $T_c$ of La4310 is always smaller than La327, in agreement with the experimental observation [1,8]. In this regard, increasing the layer number from La327 to La4310 does not enhance $T_c$. This is in sharp contrast to trilayer cuprates, which are known to exhibit the highest $T_c$ among all cuprates [77–81]. On the other hand,

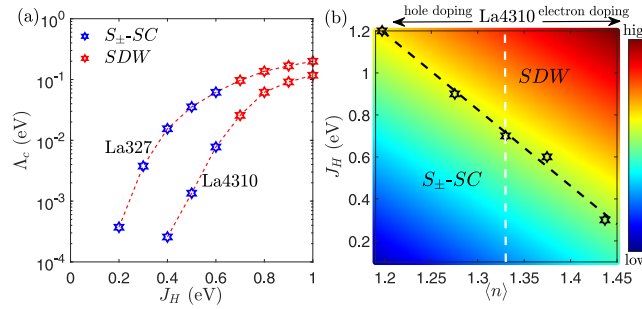


FIG. 4. (a) Phase diagram by scanning $J_H$ for both La4310 and La327. (b) Phase diagram of La4310 with respect to the filling level $\langle n \rangle$ and $J_H$, with $T_c$ qualitatively encoded by colors. In these calculations, we have used $U = 3$ eV.

the single-layer $La_2NiO_4$ (La214) is know to be insulating. Therefore, we suggest further efforts to obtain/stabilize the bilayer structure phase to search for higher-temperature superconductivity in nickelates.

We next investigate the doping effect. The phase diagram with respect to the average filling level $\langle n \rangle$ and Hund's coupling $J_H$ is plotted in Fig. 4(b), with color-scaled $T_c$ qualitatively shown. For all these fillings, SC is found to increase with $J_H$, and a large enough $J_H$ drives the system into the SDW state. In addition, electron doping is also found to enhance $T_c$. Such a tendency is consistent with the fact that with electron doping, additional low-energy fermions are created (up to the formation of an additional electronlike Fermi pocket) around $\Gamma$ with additional quasinesting with the other Fermi pockets. This doping dependence can be checked in future experiments. Finally, it would also be interesting to investigate the pressure effect, since the superconductivity was found to occur only in the high-pressure tetragonal phase. According to a recent DFT calculation [82], the $\alpha$ pocket around $\Gamma$ disappears at ambient pressure, suggesting the important role of the $\alpha$ pocket. It is also possible that the pressure plays a role to reduce the apical oxygen vacancy, which is destructive to superconductivity. We leave these to future studies.

*Conclusion*. In summary, we have constructed a minimal tight-binding model based on the nickel $3d_{3z^2-r^2}$ and $3d_{x^2-y^2}$ orbitals and investigated the electronic correlation effect using functional renormalization group for La4310 under high pressure. The spin fluctuations are found to exhibit a peculiar antiferromagnetic coupling between the two outer layers, and induce the $s_\pm$-wave superconductivity with the dominant pairings between $3d_{3z^2-r^2}$ orbitals both in the inner plane and between the two outer planes. The calculated $T_c$ in La4310 is systematically lower than in La327, suggesting La327 as the most promising candidate for higher $T_c$ in the various families of nickelates.

*Acknowledgment.* This work is supported by National Key R&D Program of China (Grant No. 2022YFA1403201), National Natural Science Foundation of China (Grants No. 12374147, No. 12274205, No. 12074213, No. 92365203, No. 11874205, and No. 11574108), and Major Basic Program of Natural Science Foundation of Shandong Province (Grant No. ZR2021ZD01).

[1] H. Sun, M. Huo, X. Hu, J. Li, Z. Liu, Y. Han, L. Tang, Z. Mao, P. Yang, B. Wang, J. Cheng, D.-X. Yao, G.-M. Zhang, and M. Wang, Signatures of superconductivity near 80 K in a nickelate under high pressure, Nature (London) **621**, 493 (2023).

[2] Z. Liu, M. Huo, J. Li, Q. Li, Y. Liu, Y. Dai, X. Zhou, J. Hao, Y. Lu, M. Wang, and H.-H. Wen, Electronic correlations and energy gap in the bilayer nickelate $La_3Ni_2O_7$, arXiv:2307.02950.

[3] J. Hou, P.-T. Yang, Z.-Y. Liu, J.-Y. Li, P.-F. Shan, L. Ma, G. Wang, N.-N. Wang, H.-Z. Guo, J.-P. Sun, Y. Uwatoko, M. Wang, G.-M. Zhang, B.-S. Wang, and J.-G. Cheng, Emergence of high-temperature superconducting phase in the pressurized $La_3Ni_2O_7$ crystals, Chin. Phys. Lett. **40**, 117302 (2023).

[4] Y. Zhang, D. Su, Y. Huang, H. Sun, M. Huo, Z. Shan, K. Ye, Z. Yang, R. Li, M. Smidman, M. Wang, L. Jiao, and H. Yuan, High-temperature superconductivity with zero resistance and strange-metal behaviour in $La_3Ni_2O_{7-\delta}$, Nat. Phys. (2024).

[5] M. Zhang, C. Pei, Q. Wang, Y. Zhao, C. Li, W. Cao, S. Zhu, J. Wu, and Y. Qi, Effects of pressure and doping on Ruddlesden–Popper phases $La_{n+1}Ni_nO_{3n+1}$, J. Mater. Sci. Technol. **185**, 147 (2024).

[6] Q. Li, Y.-J. Zhang, Z.-N. Xiang, Y. Zhang, X. Zhu, and H.-H. Wen, Signature of superconductivity in pressurized $La_4Ni_3O_{10}$, Chin. Phys. Lett. **41**, 017401 (2024).

[7] M. Zhang, C. Pei, X. Du, Y. Cao, Q. Wang, J. Wu, Y. Li, Y. Zhao, C. Li, W. Cao, S. Zhu, Q. Zhang, N. Yu, P. Cheng, J. Zhao, Y. Chen, H. Guo, L. Yang, and Y. Qi, Superconductivity in trilayer nickelate $La_4Ni_3O_{10}$ under pressure, arXiv:2311.07423.

[8] Y. Zhu, E. Zhang, B. Pan, X. Chen, D. Peng, L. Chen, H. Ren, F. Liu, N. Li, Z. Xing, J. Han, J. Wang, D. Jia, H. Wo, Y. Gu, Y. Gu, L. Ji, W. Wang, H. Gou, Y. Shen *et al.*, Superconductivity in trilayer nickelate $La_4Ni_3O_{10}$ single crystals, arXiv:2311.07353.

[9] N. Yuan, A. Elghandour, J. Arneth, K. Dey, and R. Klingeler, High-pressure crystal growth and investigation of the metal-to-metal transition of Ruddlesden–Popper trilayer nickelates $La_4Ni_3O_{10}$, J. Cryst. Growth **627**, 127511 (2024).

[10] J. Li, C.-Q. Chen, C. Huang, Y. Han, M. Huo, X. Huang, P. Ma, Z. Qiu, J. Chen, X. Hu, L. Chen, T. Xie, B. Shen, H. Sun, D. Yao, and M. Wang, Structural transition, electric transport, and electronic structures in the compressed trilayer nickelate $La_4Ni_3O_{10}$, Sci. China: Phys., Mech. Astron., (2024).

[11] A. A. C. Alvarez, S. Petit, L. Iglesias, M. Bibes, W. Prellier, and J. Varignon, Electron-phonon mediated superconductivity in $R_6Ni_5O_{12}$ nickel oxides, arXiv:2311.13674.

[12] G. Wang, N. Wang, Y. Wang, L. Shi, X. Shen, J. Hou, H. Ma, P. Yang, Z. Liu, H. Zhang, X. Dong, J. Sun, B. Wang, K. Jiang, J. Hu, Y. Uwatoko, and J. Cheng, Observation of high-temperature superconductivity in the high-pressure tetragonal phase of $La_2PrNi_2O_{7-\delta}$, arXiv:2311.08212.

[13] L. Wang, Y. Li, S. Xie, F. Liu, H. Sun, C. Huang, Y. Gao, T. Nakagawa, B. Fu, B. Dong, Z. Cao, R. Yu, S. I. Kawaguchi, H. Kadobayashi, M. Wang, C. Jin, H. Kwang Mao, and H. Liu, Structure responsible for the superconducting state in $La_3Ni_2O_7$ at high-pressure and low-temperature conditions, J. Am. Chem. Soc. **146**, 7506 (2024).

[14] Y. Zhou, J. Guo, S. Cai, H. Sun, P. Wang, J. Zhao, J. Han, X. Chen, Q. Wu, Y. Ding, M. Wang, T. Xiang, H. Kwang Mao, and L. Sun, Evidence of filamentary superconductivity in pressurized $La_3Ni_2O_7$ single crystals, arXiv:2311.12361.

[15] T. Cui, S. Choi, T. Lin, C. Liu, G. Wang, N. Wang, S. Chen, H. Hong, D. Rong, Q. Wang, Q. Jin, J.-O. Wang, L. Gu, C. Ge, C. Wang, J. G. Cheng, Q. Zhang, L. Si, K.-J. Jin, and E.-J. Guo, Strain-mediated phase crossover in Ruddlesden–Popper nickelates, Commun. Mater. **5**, 32 (2024).

[16] K. Chen, X. Liu, J. Jiao, M. Zou, C. Jiang, X. Li, Y. Luo, Q. Wu, N. Zhang, Y. Guo, and L. Shu, Evidence of spin density waves in $La_3Ni_2O_{7-\delta}$, Phys. Rev. Lett. **132**, 256503 (2024).

[17] X. Chen, J. Zhang, A. S. Thind, S. Sharma, H. LaBollita, G. Peterson, H. Zheng, D. P. Phelan, A. S. Botana, R. F. Klie, and J. F. Mitchell, Polymorphism in Ruddlesden–Popper $La_3Ni_2O_7$: Discovery of a hidden phase with distinctive layer stacking, J. Am. Chem. Soc. **146**, 3640 (2024).

[18] P. Puphal, P. Reiss, N. Enderlein, Y.-M. Wu, G. Khaliullin, V. Sundaramurthy, T. Priessnitz, M. Knauft, L. Richter, M. Isobe, P. A. van Aken, H. Takagi, B. Keimer, Y. E. Suyolcu, B. Wehinger, P. Hansmann, and M. Hepting, Unconventional crystal structure of the high-pressure superconductor $La_3Ni_2O_7$, arXiv:2312.07341.

[19] H. Wang, L. Chen, A. Rutherford, H. Zhou, and W. Xie, Long-range structural order in a hidden phase of Ruddlesden–Popper bilayer nickelate $La_3Ni_2O_7$, Inorg. Chem. **63**, 5020 (2024).

[20] M. Kakoi, T. Oi, Y. Ohshita, M. Yashima, K. Kuroki, Y. Adachi, N. Hatada, T. Uda, and H. Mukuda, Multiband metallic ground state in multilayered nickelates $La_3Ni_2O_7$ and $La_4Ni_3O_{10}$ revealed by $^{139}$La -NMR at ambient pressure, J. Phys. Soc. Jpn. **93**, 053702 (2024).

[21] T. Yamaguchi, M. Furo, Y. Sakai, T. Nishikubo, H. Hojo, M. Azuma, K. Oka, D. Mori, Y. Inaguma, M. Mizumaki, K. Yamamoto, J. Kuneš, T. Mizokawa, and A. Hariki, Mechanism of intermetallic charge transfer and bond disproportionation in $BiNiO_3$ and $PbNiO_3$ revealed by hard x-ray photoemission spectroscopy, Phys. Rev. B **109**, 205131 (2024).

[22] M. Xu, S. Huyan, H. Wang, S. L. Bud'ko, X. Chen, X. Ke, J. F. Mitchell, P. C. Canfield, J. Li, and W. Xie, Pressure-dependent "insulator-metal-insulator" behavior in Sr-doped $La_3Ni_2O_7$, arXiv:2312.14251.

[23] Z. Dong, M. Huo, J. Li, J. Li, P. Li, H. Sun, L. Gu, Y. Lu, M. Wang, Y. Wang, and Z. Chen, Visualization of oxygen vacancies and self-doped ligand holes in $La_3Ni_2O_{7-\delta}$, Nature (London) (2024).

[24] E. F. Talantsev and V. V. Chistyakov, Debye temperature, electron-phonon coupling constant, and microcrystalline strain in highly-compressed $La_3Ni_2O_{7-\delta}$, arXiv:2401.00804.

[25] B. Geisler, L. Fanfarillo, J. J. Hamlin, G. R. Stewart, R. G. Hennig, and P. J. Hirschfeld, Optical properties and electronic correlations in $La_3Ni_2O_{7-\delta}$ bilayer nickelates under high pressure, arXiv:2401.04258.

[26] Z. Luo, X. Hu, M. Wang, W. Wú, and D.-X. Yao, Bilayer two-orbital model of $La_3Ni_2O_7$ under pressure, Phys. Rev. Lett. **131**, 126001 (2023).

[27] Q.-G. Yang, D. Wang, and Q.-H. Wang, Possible $s_{\pm}$-wave superconductivity in $La_3Ni_2O_7$, Phys. Rev. B **108**, L140505 (2023).

[28] Y. Zhang, L.-F. Lin, A. Moreo, and E. Dagotto, Electronic structure, dimer physics, orbital-selective behavior, and magnetic tendencies in the bilayer nickelate superconductor $La_3Ni_2O_7$ under pressure, Phys. Rev. B **108**, L180510 (2023).

[29] H. Sakakibara, N. Kitamine, M. Ochi, and K. Kuroki, Possible high $T_c$ superconductivity in $La_3Ni_2O_7$ under high pressure through manifestation of a nearly-half-filled bilayer Hubbard model, Phys. Rev. Lett. **132**, 106002 (2024).

[30] Y. Gu, C. Le, Z. Yang, X. Wu, and J. Hu, Effective model and pairing tendency in bilayer ni-based superconductor $La_3Ni_2O_7$, arXiv:2306.07275.

[31] V. Christiansson, F. Petocchi, and P. Werner, Correlated electronic structure of $La_3Ni_2O_7$ under pressure, Phys. Rev. Lett. **131**, 206501 (2023).

[32] D. A. Shilenko and I. V. Leonov, Correlated electronic structure, orbital-selective behavior, and magnetic correlations in double-layer $La_3Ni_2O_7$ under pressure, Phys. Rev. B **108**, 125105 (2023).

[33] Y. Shen, M. Qin, and G.-M. Zhang, Effective Bi-layer model Hamiltonian and density-matrix renormalization group study for the high-$T_c$ superconductivity in $La_3Ni_2O_7$ under high pressure, Chin. Phys. Lett. **40**, 127401 (2023).

[34] W. Wú, Z. Luo, D.-X. Yao, and M. Wang, Superexchange and charge transfer in the nickelate superconductor $La_3Ni_2O_7$ under pressure, Sci. China: Phys. Mech. Astron. **67**, 117402 (2024).

[35] Y. Cao and Y.-F. Yang, Flat bands promoted by Hund's rule coupling in the candidate double-layer high-temperature superconductor $La_3Ni_2O_7$, Phys. Rev. B **109**, L081105 (2024).

[36] X. Chen, P. Jiang, J. Li, Z. Zhong, and Y. Lu, Critical charge and spin instabilities in superconducting $La_3Ni_2O_7$, arXiv:2307.07154.

[37] Y.-B. Liu, J.-W. Mei, F. Ye, W.-Q. Chen, and F. Yang, $s^{\pm}$-wave pairing and the destructive role of apical-oxygen deficiencies in $La_3Ni_2O_7$ under pressure, Phys. Rev. Lett. **131**, 236002 (2023).

[38] C. Lu, Z. Pan, F. Yang, and C. Wu, Interlayer coupling driven high-temperature superconductivity in $La_3Ni_2O_7$ under pressure, Phys. Rev. Lett. **132**, 146002 (2024).

[39] Y. Zhang, L.-F. Lin, A. Moreo, T. A. Maier, and E. Dagotto, Structural phase transition, $s_{\pm}$-wave pairing and magnetic stripe order in the bilayered nickelate superconductor $La_3Ni_2O_7$ under pressure, Nat. Commun. **15**, 2470 (2024).

[40] H. Oh and Y.-H. Zhang, Type-II $t$-$J$ model and shared superexchange coupling from Hund's rule in superconducting $La_3Ni_2O_7$, Phys. Rev. B **108**, 174511 (2023).

[41] X.-Z. Qu, D.-W. Qu, J. Chen, C. Wu, F. Yang, W. Li, and G. Su, Bilayer $t$-$J$-$J_{\perp}$ model and magnetically mediated pairing in the pressurized nickelate $La_3Ni_2O_7$, Phys. Rev. Lett. **132**, 036502 (2024).

[42] Y.-F. Yang, G.-M. Zhang, and F.-C. Zhang, Interlayer valence bonds and two-component theory for high-$T_c$ superconductivity of $La_3Ni_2O_7$ under pressure, Phys. Rev. B **108**, L201108 (2023).

[43] F. Lechermann, J. Gondolf, S. Bötzel, and I. M. Eremin, Electronic correlations and superconducting instability in $La_3Ni_2O_7$ under high pressure, Phys. Rev. B **108**, L201121 (2023).

[44] Z. Liao, L. Chen, G. Duan, Y. Wang, C. Liu, R. Yu, and Q. Si, Electron correlations and superconductivity in $La_3Ni_2O_7$ under pressure tuning, Phys. Rev. B **108**, 214522 (2023).

[45] K. Jiang, Z. Wang, and F.-C. Zhang, High-temperature superconductivity in $La_3Ni_2O_7$, Chin. Phys. Lett. **41**, 017402 (2024).

[46] H. Liu, C. Xia, S. Zhou, and H. Chen, Role of crystal-field-splitting and long-range-hoppings on superconducting pairing symmetry of $La_3Ni_2O_7$, arXiv:2311.07316.

[47] G. Heier, K. Park, and S. Y. Savrasov, Competing $d_{xy}$ and $s_{\pm}$ pairing symmetries in superconducting $La_3Ni_2O_7$: LDA+FLEX calculations, Phys. Rev. B **109**, 104508 (2024).

[48] Z. Luo, B. Lv, M. Wang, W. Wú, and D.-X. Yao, High-$T_c$ superconductivity in $La_3Ni_2O_7$ based on the bilayer two-orbital $t$-$J$ model, arXiv:2308.16564.

[49] J. Huang, Z. D. Wang, and T. Zhou, Impurity and vortex states in the bilayer high-temperature superconductor $La_3Ni_2O_7$, Phys. Rev. B **108**, 174501 (2023).

[50] Y. Zhang, L.-F. Lin, A. Moreo, T. A. Maier, and E. Dagotto, Trends in electronic structures and $s_{\pm}$-wave pairing for the rare-earth series in bilayer nickelate superconductor $R_3Ni_2O_7$, Phys. Rev. B **108**, 165141 (2023).

[51] Y.-H. Tian, Y. Chen, J.-M. Wang, R.-Q. He, and Z.-Y. Lu, Correlation effects and concomitant two-orbital $s_{\pm}$-wave superconductivity in $La_3Ni_2O_7$ under high pressure, Phys. Rev. B **109**, 165154 (2024).

[52] Q. Qin and Y.-F. Yang, High-$T_c$ superconductivity by mobilizing local spin singlets and possible route to higher $T_c$ in pressurized $La_3Ni_2O_7$, Phys. Rev. B **108**, L140504 (2023).

[53] H. Sakakibara, M. Ochi, H. Nagata, Y. Ueki, H. Sakurai, R. Matsumoto, K. Terashima, K. Hirose, H. Ohta, M. Kato, Y. Takano, and K. Kuroki, Theoretical analysis on the possibility of superconductivity in a trilayer Ruddlesden-Popper nickelate $La_4Ni_3O_{10}$ under pressure and its experimental examination: Comparison with $La_3Ni_2O_7$, Phys. Rev. B **109**, 144511 (2024).

[54] S. Ryee, N. Witt, and T. O. Wehling, Critical role of interlayer dimer correlations in the superconductivity of $La_3Ni_2O_7$, arXiv:2310.17465.

[55] Z. Ouyang, J.-M. Wang, J.-X. Wang, R.-Q. He, L. Huang, and Z.-Y. Lu, Hund electronic correlation in $La_3Ni_2O_7$ under high pressure, Phys. Rev. B **109**, 115114 (2024).

[56] W.-X. Chang, S. Guo, Y.-Z. You, and Z.-X. Li, Fermi surface symmetric mass generation: A quantum Monte-Carlo study, arXiv:2311.09970.

[57] X.-Z. Qu, D.-W. Qu, W. Li, and G. Su, Roles of Hund's rule and hybridization in the two-orbital model for high-$T_c$ superconductivity in the bilayer nickelate, arXiv:2311.12769.

[58] Y.-Y. Zheng and W. Wú, Superconductivity in the bilayer two-orbital Hubbard model, arXiv:2312.03605.

[59] Y. Wang, K. Jiang, Z. Wang, F.-C. Zhang, and J. Hu, Electronic structure and superconductivity in bilayer $La_3Ni_2O_7$, arXiv:2401.15097.

[60] M. Kakoi, T. Kaneko, H. Sakakibara, M. Ochi, and K. Kuroki, Pair correlations of the hybridized orbitals in a ladder model for the bilayer nickelate $La_3Ni_2O_7$, Phys. Rev. B **109**, L201124 (2024).

[61] Z. Fan, J.-F. Zhang, B. Zhan, D. Lv, X.-Y. Jiang, B. Normand, and T. Xiang, Superconductivity in nickelate and cuprate superconductors with strong bilayer coupling, arXiv:2312.17064.

[62] P. W. Anderson, The resonating valence bond state in $La_2CuO_4$ and superconductivity, Science **235**, 1196 (1987).

[63] F. C. Zhang and T. M. Rice, Effective Hamiltonian for the superconducting Cu oxides, Phys. Rev. B **37**, 3759 (1988).

[64] W.-S. Wang, Y.-Y. Xiang, Q.-H. Wang, F. Wang, F. Yang, and D.-H. Lee, Functional renormalization group and variational Monte Carlo studies of the electronic instabilities in graphene near 1/4 doping, Phys. Rev. B **85**, 035414 (2012).

[65] W.-S. Wang, Z.-Z. Li, Y.-Y. Xiang, and Q.-H. Wang, Competing electronic orders on kagome lattices at van Hove filling, Phys. Rev. B **87**, 115135 (2013).

[66] Q.-K. Tang, L. Yang, D. Wang, F.-C. Zhang, and Q.-H. Wang, Spin-triplet $f$-wave pairing in twisted bilayer graphene near 1/4-filling, Phys. Rev. B **99**, 094521 (2019).

[67] G. Kresse and J. Furthmüller, Efficient iterative schemes for *ab initio* total-energy calculations using a plane-wave basis set, Phys. Rev. B **54**, 11169 (1996).

[68] P. E. Blöchl, Projector augmented-wave method, Phys. Rev. B **50**, 17953 (1994).

[69] J. P. Perdew, K. Burke, and M. Ernzerhof, Generalized gradient approximation made simple, Phys. Rev. Lett. **77**, 3865 (1996).

[70] N. Marzari and D. Vanderbilt, Maximally localized generalized Wannier functions for composite energy bands, Phys. Rev. B **56**, 12847 (1997).

[71] I. Souza, N. Marzari, and D. Vanderbilt, Maximally localized Wannier functions for entangled energy bands, Phys. Rev. B **65**, 035109 (2001).

[72] G. Pizzi, V. Vitale, R. Arita, S. Blügel, F. Freimuth, G. Géranton, M. Gibertini, D. Gresch, C. Johnson, T. Koretsune, J. Ibañez-Azpiroz, H. Lee, J.-M. Lihm, D. Marchand, A. Marrazzo, Y. Mokrousov, J. I. Mustafa, Y. Nohara, Y. Nomura, L. Paulatto *et al.*, Wannier90 as a community code: New features and applications, J. Phys.: Condens. Matter **32**, 165902 (2020).

[73] C. Castellani, C. R. Natoli, and J. Ranninger, Magnetic structure of $V_2O_3$ in the insulating phase, Phys. Rev. B **18**, 4945 (1978).

[74] H. LaBollita, J. Kapeghian, M. R. Norman, and A. S. Botana, Electronic structure and magnetic tendencies of trilayer $La_4Ni_3O_{10}$ under pressure: Structural transition, molecular orbitals, and layer differentiation, Phys. Rev. B **109**, 195151 (2024).

[75] Y. Zhang, L.-F. Lin, A. Moreo, T. A. Maier, and E. Dagotto, Prediction of $s^{\pm}$-wave superconductivity enhanced by electronic doping in trilayer nickelates $La_4Ni_3O_{10}$ under pressure, arXiv:2402.05285.

[76] J. Zhang, D. Phelan, A. Botana, Y.-S. Chen, H. Zheng, M. Krogstad, S. G. Wang, Y. Qiu, J. Rodriguez-Rivera, R. Osborn *et al.*, Intertwined density waves in a metallic nickelate, Nat. Commun. **11**, 6003 (2020).

[77] A. Schilling, M. Cantoni, J. D. Guo, and H. R. Ott, Superconductivity above 130 K in the Hg-Ba-Ca-Cu-O system, Nature (London) **363**, 56 (1993).

[78] L. Gao, Y. Y. Xue, F. Chen, Q. Xiong, R. L. Meng, D. Ramirez, C. W. Chu, J. H. Eggert, and H. K. Mao, Superconductivity up to 164 K in $HgBa_2Ca_{m-1}Cu_mO_{2m+2+\delta}$ ($m = 1$, 2, and 3) under quasihydrostatic pressures, Phys. Rev. B **50**, 4260 (1994).

[79] B. Scott, E. Suard, C. Tsuei, D. Mitzi, T. McGuire, B.-H. Chen, and D. Walker, Layer dependence of the superconducting transition temperature of $HgBa_2Ca_{n-1}Cu_nO_{2n+2+\delta}$, Phys. C: Superconductivity **230**, 239 (1994).

[80] I. G. Kuzemskaya, A. L. Kuzemsky, and A. A. Cheglokov, Superconducting properties of the family of mercurocuprates and role of layered structure, J. Low Temp. Phys. **118**, 147 (2000).

[81] A. Iyo, Y. Tanaka, H. Kito, Y. Kodama, P. M. Shirage, D. D. Shivagan, H. Matsuhata, K. Tokiwa, and T. Watanabe, $T_c$ vs $n$ relationship for multilayered high-$T_c$ superconductors, J. Phys. Soc. Jpn. **76**, 094711 (2007).

[82] Z. Luo, C.-Q. Chen, M. Wang, W. Wú, and D.-X. Yao, Trilayer multi-orbital models of $La_4Ni_3O_{10}$, arXiv:2402.07196.